A Theoretical Study of the Interaction of HCl with Crystalline NAT

Yves A. Mantz,[†] Franz M. Geiger,[‡] Luisa T. Molina, and Mario J. Molina

Department of Earth, Atmospheric, and Planetary Sciences and of Chemistry, Massachusetts Institute of Technology, Cambridge, Massachusetts 02139-4307

Bernhardt L. Trout*

Department of Chemical Engineering, Massachusetts Institute of Technology, Cambridge, Massachusetts 02139-4307

Received: December 10, 2001; In Final Form: April 4, 2002

Using density-functional-plane-wave-based and localized-orbital computational methods, we systematically examine the binding of molecular HCl at a variety of surface sites on crystalline nitric acid trihydrate (NAT), a step preceding the chlorine activation reactions that contribute to the depletion of stratospheric ozone at high latitudes. We pay particular attention to the role played by surface dangling (non-hydrogen-bonding) OH groups. After optimizing six low index faces, we find that NAT(001) and (00$\bar{1}$) faces are thermodynamically the most stable. Only one surface site on the (001) face, with one nearby dangling OH group, exhibits a high affinity for HCl. At this binding site, adsorbed HCl forms a strong H···O hydrogen bond with an NO_3^- ion and a weaker Cl···H hydrogen bond with a nearby H_2O molecule. The interaction energy and enthalpy at 190 K corrected for zero-point energies are 23 and 25 kJ/mol, respectively. The presence of one strong binding site per simulation cell, versus at least three previously reported on the (0001) face of ice I*h* (Mantz, Y. A.; Geiger, F. M.; Molina, L. T.; Molina, M. J.; Trout, B. L. *J. Phys. Chem. A* **2000**, *105*, 7037), leads to a prediction of a lower HCl surface coverage on NAT than on ice, qualitatively consistent with experiments conducted on these surfaces. Additionally, we present kinetic and thermodynamic evidence that molecular HCl, adsorbed near one or two dangling OH groups, does not dissociate on NAT. By contrast, molecularly adsorbed HCl likely dissociates when interacting strongly with two dangling OH group on the ice I*h* (0001) face as reported in previously published theoretical studies (Svanberg, M.; Pettersson, J. B. C.; Bolton, K. *J. Phys. Chem. A* **2000**, *104*, 5787; Mantz, Y. A.; Geiger, F. M.; Molina, L. T.; Molina, M. J.; Trout, B. L. *Chem. Phys. Lett.* **2001**, *348*, 285).

I. Introduction

The surfaces of polar stratospheric cloud (PSC) particles, formed during the cold polar winter, are now widely recognized to catalyze halogen activation reactions, e.g., reactions 1−3, which result in the production of "active" halogen compounds, e.g., Cl_2 and HOCl.[1−4] These "active" compounds are photolyzed by sunlight during early spring to yield radicals that efficiently destroy polar stratospheric ozone via gas-phase catalytic cycles.[1−4] Two general types of solid PSC particles are thought to exist composed primarily of nitric acid trihydrate (NAT) crystals (Type Ia PSCs) and of ice I*h* crystals (Type II PSCs).[1,2] Another significant form of PSC is composed of spherical droplets of supercooled $HNO_3/H_2SO_4/H_2O$ ternary solutions (Type Ib PSCs).[1,2] One area of research interest in the atmospheric sciences is the molecular-level elucidation of chlorine-activation mechanisms, i.e., reactions 1−3, on solid PSC particle surfaces.

$$ClONO_2(g) + H_2O(s) \xrightarrow{PSC} HOCl(g,ads) + HNO_3(ads) \quad (1)$$

$$HOCl(ads) + HCl(ads) \xrightarrow{PSC} Cl_2(g) + H_2O(s) \quad (2)$$

$$ClONO_2(g) + HCl(ads) \xrightarrow{PSC} Cl_2(g) + HNO_3(s) \quad (3)$$

Chlorine activation on water-ice surfaces is currently being investigated most actively, due to the comparatively simple chemical composition of Type II PSC particles, which consist mainly of only one chemical species, H_2O. However, the detailed surface structure of water-ice crystals under stratospheric conditions, including, e.g., the degree and extent of reconstruction and surface disordering,[5] the surface density of dangling (non-hydrogen-bonding) OH groups,[6] and the occurrence frequency of defects,[5] is not well established. Consequently, the relative importance of the several proposed mechanisms for reactions 1[7−10] and 3[11−23] on Type II PSCs is still being debated. For reaction 1, experimental findings on ice surfaces include cleavage of the Cl−ONO_2 bond,[24] the controversial "presence" of an H_2OCl^+ intermediate,[8,10,25,26] and slow (∼minutes) autocatalytic production of HOCl dependent on $ClONO_2$ exposure;[7] and for reaction 3, experiments show the absence of surface HOCl[7] and prompt (∼tens of milliseconds) appearance of Cl_2.[27] For reaction 3, surface dangling

* Corresponding author. Fax: 617-258-8224. E-mail: trout@mit.edu.
[†] Current address: IBM T. J. Watson Research Center, Route 134 & P.O. Box 218, Yorktown Heights, NY 10598-0218.
[‡] Current address: Department of Chemistry, Northwestern University, Evanston, IL 60208-3113.

10.1021/jp0144754 CCC: $22.00
Published on Web 07/09/2002

OH groups likely play a role in the formation of an $H^{\delta+}\cdots Cl^{\delta-}$ contact ion pair at sites on the ice surface which are reactive toward $Cl^{\delta+}NO_3^{\delta-}$(g), based on theoretical findings from our group and others.[13,16,17,19,20]

Progress toward understanding chlorine activation on Type Ia PSC particle surfaces, thought to be composed primarily of thermodynamically stable NAT crystals,[28−30] is not as advanced as that on Type II PSC particles, and the mechanism of reaction 1 on NAT is presently unclear. Experimentally, the efficiency of reaction 1 on NAT at a given temperature depends strongly on the relative humidity.[3,4] If the partial pressure of water vapor is adjusted to approach that of ice, the measured efficiency of rection 1 on NAT approaches ∼1% of that measured on ice, but as the relative humidity is decreased, the efficiency of reaction 1 on NAT decreases by 2 orders of magnitude.[31] For a given partial pressure of water vapor, the temperature dependence of reaction 1 on NAT may also be weakly negative.[32] Both dependences might be explained by the presence of H_2O molecules adsorbed at the "neat" NAT surface.[32,33] Alternatively, the explanation may lie in a partially disordered "quasi-liquid" layer formed by incorporated H_2O molecules, which may depend at a given temperature on the ambient H_2O and HNO_3 partial pressures.[15] For a specified set of conditions, either "H_2O-rich" or "HNO_3-rich" NAT in equilibrium with ice I*h* or nitric acid monohydrate (NAM), respectively, or an intermediate form may be present.[15] The *bulk* chemical composition of these different forms differs by arbitrarily small amounts from the stoichiometric 3:1 ratio, but the *surface* chemical compositions may be very different, a hypothesis that is compatible with the Gibbs phase rule.

Experiments indicate that the efficiency of reaction 3 on NAT also exhibits a strong dependence on the relative humidity/H_2O partial pressure, independent of the partial pressure of HCl: The dependences observed in flow-tube experiments by Abbatt and Molina[31] (202 K, $1-9\times10^{-6}$ Torr $ClONO_2$, $4-10\times10^{-6}$ Torr HCl) and Hanson and Ravishankara[34] (191 K, $\sim2.5-5\times10^{-8}$ Torr $ClONO_2$, $5-10\times10^{-8}$ Torr HCl) are quantitatively very similar despite the factor of 100 difference in partial pressures of HCl used. The (essentially identical) dependence on relative humidity observed in both experiments may be due to the varying affinity of HCl for the NAT surface depending on the availability of coadsorbed H_2O molecules. However, attempts to model this dependence using, e.g., a simple coadsorption approach,[35] have not been successful.[36] Similar to the H_2O partial pressure dependence of reaction 3 on NAT, reaction 3 on NAT also depends on the HCl partial pressure at a given relative humidity: Abbatt and Molina[31] observe an enhancement by a factor of 4 of the efficiency of reaction 3 on "HNO_3-rich" NAT (H_2O partial pressure of 2.5×10^{-4} Torr) when the partial pressure of HCl is increased from 1.5×10^{-5} to 8×10^{-5} Torr. The preceding summary of chlorine activation on NAT suggests the need for additional careful experimental studies of rections 1−3 on NAT over a range of stratospherically relevant conditions of temperature and HCl and H_2O partial pressures.

A key step preceding reaction 3 on NAT is the interaction of HCl with the NAT surface. An HCl surface coverage of 8×10^{13} to 5×10^{14} molecule/cm^2 was measured by Chu et al.[37] using an HCl partial pressure of 4.5×10^{-7} Torr and NAT substrates maintained at 188 K with surface compositions intermediate between "H_2O-rich" and "HNO_3-rich" forms. This range of surface coverage is comparable to that measured on water-ice surfaces, from 2×10^{13} to 4×10^{14} molecule/cm^2 (180 to ∼220 K, $10^{-9}-2\times10^{-5}$ Torr HCl).[38−40] On "HNO_3-rich" NAT, the uptake of HCl is a linear function of the HCl partial pressure, ranging from 8×10^{12} to 2×10^{14} molecule/cm^2 ($4\times10^{-6}-10^{-4}$ Torr HCl and 5×10^{-4} Torr H_2O at 202 K).[31] At stratospherically relevant HCl partial pressures ($10^{-8}-10^{-7}$ Torr HCl), a surface coverage of $10^{10}-10^{11}$ molecule/cm^2 is estimated by linear extrapolation for this surface.

The state of HCl on NAT, i.e., molecularly or dissociatively adsorbed, is not known, because neither experimental nor theoretical studies have been performed to address this issue. Heterogeneous chlorine activation reactions involving HCl on water-ice surfaces are very rapid in comparison to the prohibitively slow gas-phase rates,[4] leading in the past to the suggestion that a mechanism with a low activation energy involving at least some degree of HCl dissociation is operative on ice surfaces. By contrast, the efficiency of reaction 3 on "HNO_3-rich" NAT is enhanced relative to the gas phase but is orders of magnitude smaller than on "H_2O-rich" NAT or water ice, resulting perhaps from a less efficient mechanism with a higher activation energy that does not necessarily require the same degree of HCl dissociation as on ice surfaces, and/or from a lower reactant surface coverage.[3,4]

Theoretical studies utilizing periodic models of both the bulk and clean surface of NAM[41,42] as well as of bulk NAT[43] have provided a basis for understanding the interaction of HCl with the NAT surface and ultimately for detailed mechanistic studies of chlorine activation. While NAM is less atmospherically relevant, more extensive theoretical studies have been performed on this solid due to its smaller (and less anisotropic) unit cell and consequently greater tractability. Poshusta et al.[41] obtained the first detailed theoretical description of bulk NAM using CRYSTAL92. Based on their finding that bulk NAM is composed of weakly bound puckered layers, a surface that exposes such a puckered layer was reasoned to have the minimum surface energy and hence be most prevalent. This surface (consisting of the [001] family of planes in the nonstandard $P2_1cn$ space group) was characterized in order to predict favorable sites for physisorption and potentially important sites for surface catalysis. It was later suggested by Tóth[42] that this surface of NAM does not act catalytically, based on two sets of results using CPMD. First, from a few select geometry optimizations of HCl, $ClONO_2$, and H_2O placed initially at random positions on the (001) surface, small 0 K physisorption energies not corrected for zero-point energies were calculated (e.g., 15 kJ/mol for HCl). Second, no reasonable change in the adsorbate geometries was observed during a 0.5 ps CPMD simulation at 195 K.

It is unclear whether the findings of Tóth[42] apply as well to the crystalline NAT surface. Due to its larger unit cell size, there are very few (if any) published theoretical studies of the NAT surface or of chlorine activation on NAT surfaces; only recently have the structural, spectroscopic, and dynamic properties of bulk NAT been characterized theoretically.[43] These investigations would be relevant given the relative abundance (particularly in the Arctic) of Type Ia PSCs, which are observed at several degrees above the ice frost point. An additional caveat in performing theoretical studies on NAT is that the variety of possible adsorption sites is large (as discussed in Section IIIA). High-level ab initio approaches using cluster models representative of the variety of adsorption sites would be impractical. Furthermore, no potentials are available that are parametrized for the study of crystalline NAT under any conditions, precluding classical simulation approaches. This article represents a needed initial effort toward elucidating theoretically the mech-

TABLE 1: Optimized Geometry and Binding Energy of $HNO_3 \cdot H_2O$, and Geometries of Isolated HNO_3 and H_2O (bond lengths in Å, bond angles in degrees, binding energy in kJ/mol, and uncertainty in parentheses)

	BLYP/PW[a]			BLYP/PW[b]		MP2/6-311++G(2d,p)[c]		experiment	
parameter (Figure 1)	fixed planar	fully relaxed	HNO_3 or H_2O	fully relaxed	HNO_3 or H_2O	fully relaxed	HNO_3 or H_2O	$HNO_3 \cdot H_2O$[d]	HNO_3[e] or H_2O[f]
$r(NO_{cis})$	1.24	1.24	1.23	1.28	1.27	1.23	1.22		1.213(2)
$r(NO_{trans})$	1.22	1.22	1.22	1.26	1.26	1.21	1.21		1.198(2)
$r(N-O'H)$	1.43	1.43	1.49	1.45	1.49	1.38	1.41		1.410(2)
$r(O'H)$	1.01	1.01	0.98	1.03	1.00	1.00	0.98		0.941(3)
$\angle O_{cis}NO_{trans}$	128.8	128.7	131.5			128.5	130.5		130.2(2)
$\angle O_{cis}NO'$	116.7	116.7	115.3			116.9	115.7		115.7(2)
$\angle O'NO_{trans}$	114.5	114.5	113.2			104.2	102.2		114.1(2)
$\angle NO'H$	104.4	104.1	101.8	104.1	102.3				102.6(3)
$r_w(OH)$	0.97	0.97	0.97	0.99	0.99	0.96	0.96		0.9572(3)
$\angle HOH$	106.2	106.4	104.4	105.4	103.8	106.1	104.6		104.52(5)
R	1.69	1.70				1.71		1.779(33)	
α	178.5	176.0		173.8		176.4		174.50(41)	
β	102.7	103.2				101.3		92(8)	
ϕ	45.9					49.9		30(10)	
R_{sec}	2.61	2.57				2.4		2.30	
θ	106.1	105.7				$\approx$105		119.3	
BE[g]	$-\Delta E_e^B = 35$			$-\Delta E_c^B = 32$		$-\Delta E_o^B = 41$			

[a] This work. [b] Ref 42. [c] Ref 58. [d] Ref 61. [e] Ref 62. [f] Ref 63. [g] Computed either with ($-\Delta E_o^B$) or without ($-\Delta E_e^B$) zero-point energies taken into account and with the counterpoise correction for basis set superposition error (which is equal to zero in plane-wave calculations).

anism(s) of chlorine activation and parallels that of our recent studies of HCl interacting with ice I*h*.[16,17]

II. Theoretical Approaches

A. Brief Description. For both geometry optimizations and simulations performed using the CPMD code,[44] the electronic state is described using density-functional theory with either the BLYP[45,46] or (when specified) the LDA[47] functional, atomic norm-conserving pseudopotentials,[48] and using only the Γ point for Brillouin-zone sampling. A plane-wave basis set with a 70 Ry cutoff (unless otherwise noted) is used.

The approaches implemented in CPMD for the geometry optimization of relevant test molecules, including H_2O, $(H_2O)_2$, HCl, and HNO_3 (Section IIB), and for larger systems, including $HNO_3 \cdot H_2O$ (Section IIB), bulk NAT (Section IIB), the "neat" NAT surface (Section IIIA), and HCl adsorbed on the "neat" NAT surface (Section IIIB) are described in detail elsewhere.[17] For optimizing the geometry of HCl adsorbed on the "neat" NAT surface (Section IIIB), we do not sample the $3N-6$-dimensional potential surface as thoroughly as either "simulated annealing"[49] (with a nonzero initial temperature and a scaling factor larger than 0.9 used here) or a highly methodical sampling (with respect to r, θ, and ϕ of all possible configurations of adsorbed HCl interacting with each surface site) would. Our optimizations, however, are fully converged (to local minima) within a reasonable amount of computational time. We note that $HNO_3 \cdot HCl$ isomers (Section IIIB) were optimized using Gaussian 94,[50] and a vibrational mode analysis was performed using a frequency scaling factor of 1.0119[51] which we verified yields reasonable vibrational spectra for HCl[52] and HNO_3.[53]

Three dynamical simulations using the Car-Parrinello technique[54,55] of HCl interacting with NAT (Section IIIC) were performed at a simulation temperature of 155 K, as described in our study of surface disordering of an extended surface model of ice I*h* as a function of temperature.[18] The choice of 155 K, 40 K below the typical formation temperature (195 K) of Type Ia PSCs, was made on the basis of an estimate[18] of 220 K for the melting point of an ice I*h* slab model which was not made rigorously[56] and is not considered precise.

B. Validation: Optimization of Relevant "Building Blocks" and Bulk NAT. As described elsewhere, the bond lengths and bond angles of H_2O,[57] $(H_2O)_2$,[57] and HCl[17] are predicted to within a few hundredths of an angstrom and one degree of experimental values using CPMD with the BLYP functional. In addition, results for H_2O, HNO_3, and $HNO_3 \cdot H_2O$ (Figure 1), important "building blocks" in this study, are reported in Table 1. For $HNO_3 \cdot H_2O$, geometry optimizations were performed both with the planarity of the ring constrained (by fixing the z-coordinates of all atoms except the free hydrogen of H_2O to zero) and with the ring free to relax (i.e., no constraints). These results are reported under the column headings "fixed planar" and "fully relaxed," respectively. Our computed geometries for H_2O, HNO_3, and $HNO_3 \cdot H_2O$ compare well to other theoretical predictions.[42,58-60] Our computed geometries also compare well to the experimental data for $HNO_3 \cdot H_2O$[61] (consistent with a structure that forms a planar, six-membered ring), HNO_3,[62] and H_2O.[63] For $HNO_3 \cdot H_2O$ in particular, the six-membered ring formed by our optimized structure obtained without constraints is nearly planar (with absolute deviations of z-coordinates from zero of less than 0.06 Å), while the geometry is very similar and the binding energy of 35 kJ/mol is identical to that of the constrained structure. Our predicted binding energy for $HNO_3 \cdot H_2O$ is similar to that reported by Tóth,[42] who also uses CPMD but with a smaller cutoff of 40.0 Ry and Vanderbilt ultrasoft pseudopotentials, and is slightly less than the value reported by Tao et al.[58] at the MP2 level of theory with a localized 6-311++G(2d,p) basis set and corrected for both zero-point energies and basis set superposition error. No experimental binding energy for $HNO_3 \cdot H_2O$ is available.

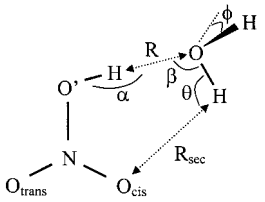

Figure 1. Labels and definitions of geometric parameters for $HNO_3 \cdot H_2O$.

The geometry of bulk crystalline NAT, modeled using a 112-atom, $1 \times 1 \times 2$ arrangement of orthorhombic unit cells[64] periodically repeated ad infinitum (Figure 2), was optimized for a few selected values of the lattice constants. As for bulk

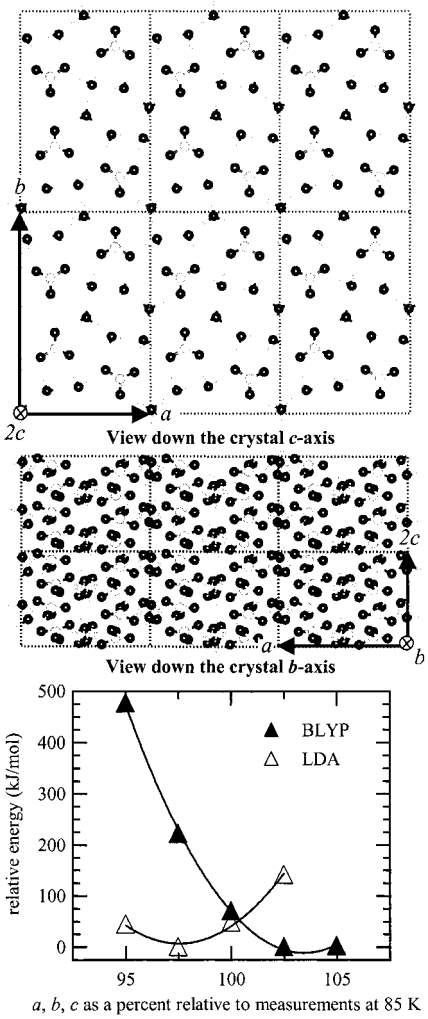

Figure 2. Six-cell periodic representations of our optimized bulk crystalline NAT simulation cell shown from orthogonal perspectives. Plotted are the energies in kJ/mol relative to the most stable simulation cell obtained with either the BLYP or LDA functional as a function of relative lattice constants.

ice I*h*,[16] fractional cutoffs ranging from 70 to 70.070 Ry (BLYP) and 70.000 to 70.052 Ry (LDA) were used in order to fix the basis set density, i.e., the number of plane waves per unit volume. For each optimization, each lattice constant was varied by the same percentage relative to the accepted experimental value at 85 K,[64] in increments of 2.5%. We point out that the initial atomic coordinates were not simply "scaled," but changed so as to preserve the space group $P2_12_12_1$ symmetry. A more thorough testing (i.e., varying *a*, *b*, and *c* independently in smaller increments) was not performed, because of computational cost. The most stable simulation cell obtained with the BLYP functional from a thermodynamic point of view is associated with lattice constants only 3.4% greater than experiment,[64] at the minimum of the best-fit ($R^2 = 0.999$) quadratic curve in Figure 2. This result is reasonable given that BLYP, as a general rule, slightly overestimates lattice constants; it overestimates by 2.6% the *c* lattice constant of bulk ice I*h*.[16] By contrast, the LDA functional generally underestimates lattice constants, as our prediction of lattice constants 97.5% of the experimental results at 85 K suggests (Figure 2).

The geometry of the BLYP-optimized simulation cell whose lattice constants are 2.6% greater than experiment[64] compares satisfactorily with X-ray diffraction data[64] (Table 2 and Figure 3). The agreement is best for intramolecular distances and angles, i.e., d_{NO} and ∠ONO, due to the fact that our lattice constants are larger than experiment, an overestimation that affects intermolecular distances and angles. Not shown in Table 2 is the fact that our calculated OH bond lengths (which correspond to predicted most probable internuclear distances) are 0.11−0.19 Å greater than the OH distances estimated from X-ray diffraction data.[64] This is explained by the fact that X-ray diffraction provides electron density distributions, the maximum of which is shifted along the OH bond relative to the position of the nuclei. (According to our calculations, the electron density is a maximum along the OH bond close to the oxygen atom). In ice I*h*, for example, the OH distances estimated from X-ray diffraction data are 0.15−0.17 Å shorter than those determined by neutron diffraction.[65] We conclude that CPMD, which was also used successfully to describe both NAM[42] as well as NAT[43] by others and to study the interaction of HCl with ice I*h* by our laboratory,[16,17] may be confidently used to study the interaction of HCl with NAT. The lowest energy simulation cells obtained with the BLYP and LDA functionals (with dimensions 9.722 Å × 15.051 Å × 7.043 Å and 9.247 Å × 14.317 Å × 6.699 Å, respectively) are our starting points for optimizing the surface.

III. Results

A. Optimization of Low Index NAT Faces, and Selection and Analysis of the (001) Face. Different families of low index faces of NAT exhibit significantly different structure and polarity characteristics, e.g., the relatively smooth (010) face consists of a top layer of H_3O^+ ions, while the jagged (100) face and the similarly rough (001) face consist of alternating H_3O^+ ions, NO_3^- ions, and H_2O molecules at the surface. A detailed study of HCl adsorption on each low index face of NAT would be extremely time-consuming, given the large variety of possible adsorption sites, and would not be necessary if it were known which faces were most prevalent. At the melting point of −18.5 °C, the growth of NAT crystals from solution occurs preferentially along the *c*-axis, suggesting that [100] and [010] families of faces might be more relevant than the [001] family for crystals grown directly from the vapor phase under polar stratospheric conditions.[64] There may, however, be a growth-rate switchover at lower temperatures, similar to that observed in ice I*h*: For ice I*h* crystals grown directly from the vapor phase, the basal (0001) face is most relevant at temperatures below about −11 °C, while the prism family of faces including [1000], [0100], and [0010] are more relevant at temperatures above −11 °C.[66,67] One reason to believe a switchover may not occur in NAT is that ice I*h* is structurally and chemically quite different. Experimental growth data as obtained for ice I*h* are needed for confirmation.

In bulk NAT, longer (and therefore weaker) hydrogen bonds typically run along the crystal *c*-axis.[64] We predict, therefore, that the smallest amount of energy will be required to expand the space between two layers along the *c*-axis, or to cleave along this direction. Consequently, the [001] family of faces, from a thermodynamic point of view, is likely prevalent. This prediction was tested by optimizing the (100), (1$\bar{0}$0), (010), (0$\bar{1}$0), (001), and (00$\bar{1}$) faces of NAT (Figures 4 and 5). Each face was modeled by adding a sufficiently large[17] surface vacuum region of 8 Å in the appropriate direction to the optimized bulk NAT simulation cell (Section IIB), applying periodic boundary conditions, and fixing underlying atoms to their bulk optimized positions in order to mimic the effects of an infinite bulk. Importantly, the same number of each chemical group (i.e., NO_3^-, H_3O^+, and H_2O) was fixed making comparison between different faces possible. Fractional cutoffs of 70.010−70.060 Ry (BLYP) and 70.004−70.050 Ry (LDA) were used in order

TABLE 2: NAT Experimental and Calculated Bulk and (001) Face Geometries (*d*'s in Å, *a*'s in degrees)

parameter (Figure 3)	experiment[a]	bulk	(001) face
d1 (d_{NO})	1.256(2)	1.28	1.28
d2	1.247(2)	1.27	1.27
d3	1.265(2)	1.29	1.29
d4 (d_{OO})	2.798(2)	2.84	2.84
d5	2.755(2)	2.76	2.77
d6	2.800(2)	2.81	2.83
d7	2.576(2)	2.60	2.59
d8	2.626(2)	2.62	2.63
d9	2.482(2)	2.50	2.52
d10	2.809(2)	2.80	2.80
a1 (∠ONO)	120.3(1)	120.3	120.3
a2	121.2(1)	121.4	121.4
a3	118.5(1)	118.4	118.3
a4 (∠NOO)	109.9(1)	114.9	114.6
a5	106.6(1)	110.9	110.9
a6	110.0(1)	112.3	112.2
a7	116.9(1)	109.2	109.2
a8 (∠OOO)	133.0(1)	138.0	138.1
a9	115.5(1)	113.6	113.1
a10	127.2(1)	126.3	126.6
a11	102.1(1)	97.5	97.6
a12	102.1(1)	105.9	105.9
a13	118.2(1)	120.2	120.3
a14	91.6(1)	91.3	91.3
a15	103.1(1)	104.3	104.0
a16	112.8(1)	113.9	113.8
a17	116.8(1)	119.7	119.5
a18	122.7(1)	121.4	120.1
a19	99.6(1)	105.7	105.6
a20	124.4(1)	121.3	121.4

[a] Ref 64.

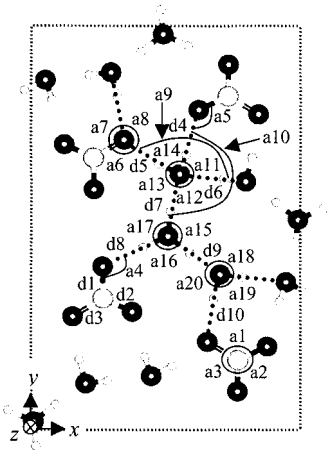

Figure 3. Labels and definitions of geometric parameters for our crystalline NAT simulation cell.

to fix the basis set density, i.e., the number of plane waves per unit volume.[16] Interestingly, during optimizations with either functional, proton transfer at the (100), ($\bar{1}$00), (010), and (0$\bar{1}$0) faces is observed (Figure 4). This occurs in order to bring closer together oppositely charged NO_3^- and H_3O^+ chemical groups. As expected, there is an energetic penalty associated with the formation of each face examined with respect to bulk NAT (Table 3); furthermore, for a given face, the penalty obtained with the LDA functional is greater than that obtained with BLYP, due to the fact that LDA typically overestimates bond strengths, whereas BLYP typically (slightly) underestimates bond energies. The surface energy of either (001) or (00$\bar{1}$) faces is smallest, as shown in Table 3, independent of functional. Consequently, out of the faces examined, we predict from a thermodynamic point of view that (001) or (00$\bar{1}$) faces are

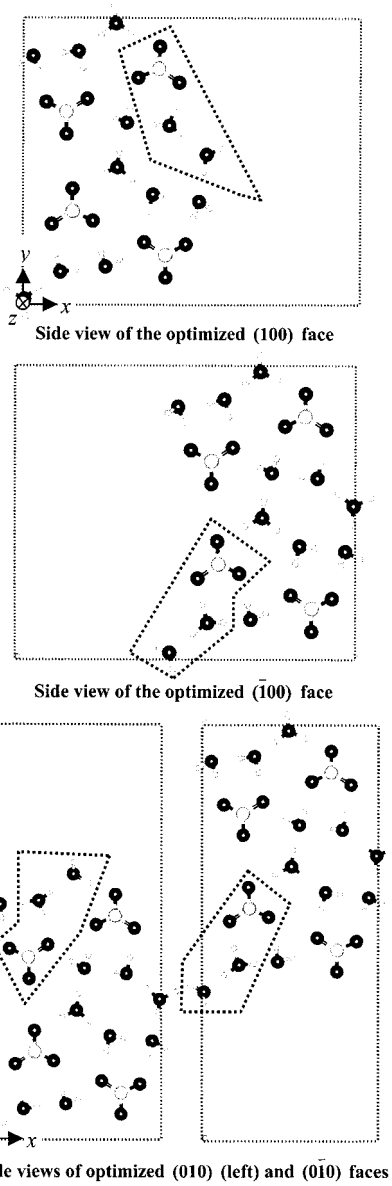

Figure 4. Simulation-cell depictions of four optimized NAT faces. Proton transfers from the surface H_3O^+ to an underlying H_2O molecule yield $NO_3^-\cdot H_3O^+\cdot H_2O$ complexes (dash-enclosed).

favored (a conclusion further supported by results in Section IIIC). This prediction does not necessarily mean that (001) or (00$\bar{1}$) faces of Type Ia PSC particles will be most prevalent in the polar stratosphere, because of the limited subset of faces examined, the role of surface defects in minimizing surface energy, and the fact that kinetic (rather than thermodynamic) barriers to growth determine relative face abundance. Furthermore, we select for detailed study HCl interacting with the (001) as opposed to the (00$\bar{1}$) face, which does not have a surface dangling OH group. Subsequently, on the basis of these results, we predict which sites on the (100), ($\bar{1}$00), (010), and (0$\bar{1}$0) faces are likely to exhibit a significant interaction with HCl and examine these sites.

The optimized geometry of the (001) face of NAT obtained with the BLYP functional is reported in Table 2. Surface reconstruction upon optimization is minor, as indicated by comparison of distances and angles to the bulk optimized structure. To predict favorable binding sites for HCl on the (001) face and compare electronic properties of the surface and bulk, electron localization function[68] (*ELF*) isosurfaces were computed for the bulk (without vacuum region) and surface (with vacuum

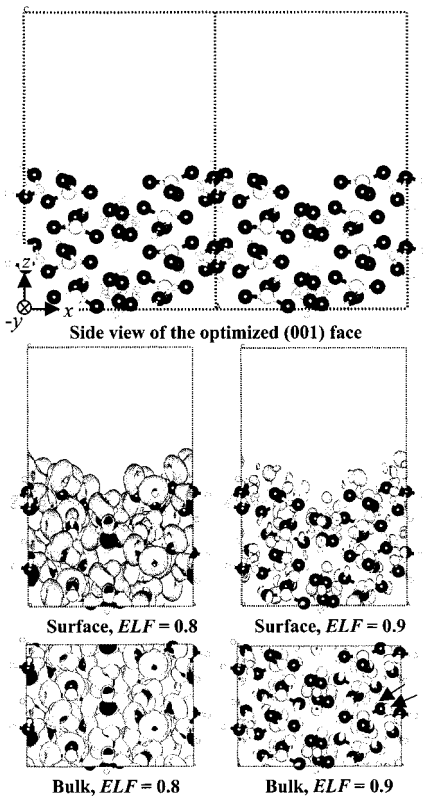

Figure 5. Two-simulation-cell periodic representation of the optimized NAT(001) face, and *ELF* isosurfaces for this face and bulk.

TABLE 3: Calculated Destabilization Energies per Unit Area of Optimized Faces Relative to Bulk NAT

		cell dimensions				
face	functional	*x* (Å)	*y* (Å)	*z* (Å)	area (Å^2)	ΔE (kJ/mol/Å^2)
(100)	BLYP	17.72	15.05	7.04	106	4.49
	LDA	17.25	14.32	6.70	96	6.54
($\bar{1}$00)	BLYP	17.72	15.05	7.04	106	4.49
	LDA	17.25	14.32	6.70	96	6.54
(010)	BLYP	9.72	23.05	7.04	68	3.14
	LDA	9.25	22.32	6.70	62	5.38
(0$\bar{1}$0)	BLYP	9.72	23.05	7.04	68	3.11
	LDA	9.25	22.32	6.70	62	5.38
(001)	BLYP	9.72	15.05	15.04	146	0.43
	LDA	9.25	14.32	14.70	132	2.40
(00$\bar{1}$)	BLYP	9.72	15.05	15.04	146	0.43
	LDA	9.25	14.32	14.70	132	2.40

region) NAT models depicted in Figures 2 and 5, respectively (each with 112 atoms). The *ELF*, defined elsewhere,[68] is a measure of electron localization and does *not* depend on performing a unitary transformation to generate localized orbitals; such transformations of the (generally delocalized) canonical orbitals (of Hartree−Fock theory) are done in order to give a more intuitive feel for bonding but are nonunique and may result in qualitatively different views of certain bonding situations (i.e., the dichotomy between "$\sigma-\pi$" and "bent" multiple bonds).[68] The *ELF* ranges between 0 and 1, where a value of one indicates that the electron is most localized. Selected isosurfaces (*ELF* = 0.8 and 0.9) for the bulk and (001) face are shown in Figure 5. The *ELF* = 0.8 isosurfaces are halo-shaped and symmetrically centered about the oxygen atoms within the crystal bulk (as observed in liquid water),[69] but not near the surface where they protrude into the vacuum in order to minimize electrostatic repulsions. The *ELF* = 0.9 isosurfaces reveal the presence of two lobes on the oxygen atoms each corresponding to an electron lone pair, as pointed out with black arrows on one oxygen atom in Figure 5. Extending our analysis

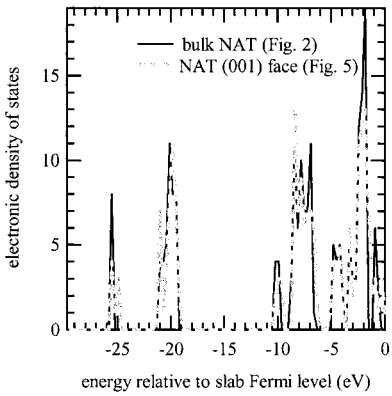

Figure 6. Density of states calculated for the NAT(001) face and bulk. A bin size of 0.3 eV was used.

of electronic properties, we note that the total electronic density of states (Figure 6) for bulk NAT (Figure 2) and the (001) face (Figure 5) are similar. This is not surprising, given that the surface model (with 56 fixed atoms) includes a relatively high number of bulk molecules. The separation (of 9 eV) between groups of bands is characteristic of an insulating ionic solid; further insight may be gained by comparing Figure 6 to the qualitatively similar density of states obtained for NAM by Poshusta et al.[41]

B. Geometry and Energetics of Molecular HCl Adsorbed on NAT and Coverage Dependence. Optimized geometries and binding energies for HCl in 54 different initial configurations on the NAT(001) face (as modeled in Section IIIA) were calculated. A systematic procedure for selecting initial configurations was adopted. First, complexes with HCl oriented approximately perpendicular to each chemical group (such as NO_3^- or H_2O) that comprise the (001) surface were examined. Configurations with the $Cl^{\delta-}$ of HCl interacting (as opposed to the $H^{\delta+}$ of HCl interacting) with the surface were concluded to be at best only weakly binding, based on a few trial optimizations and results for HCl interacting with ice I*h*,[20,70] and were thus ruled out. Also ruled out were configurations resulting in overcrowding or juxtaposition of like (atomic) charges. The HCl molecule was oriented always with the (slightly) positive end toward the surface, and positioned on the basis of the charge of the interacting chemical group; for neutral H_2O, typical results[17] for the $HCl{\cdot}H_2O$ complex were used ($d_{H\cdots O} \sim 1.9$ Å and $\angle ClHO \sim 180°$), while a somewhat longer or shorter hydrogen bond was chosen when the interacting chemical group was H_3O^+ or NO_3^-, respectively. After all of the plausible so-called "90° orientations" were optimized, complexes with HCl oriented *roughly* 45° to each chemical group were sampled (i.e., with the $Cl^{\delta-}$ of HCl able to form a hydrogen bond with the same or a different chemical group), following the same criteria. Chemical groups buried within the slab were ignored and fixed to bulk optimized positions; the other 56 atoms of the slab were allowed to relax.

The 18 different configurations (out of 54 tested) resulting in a binding energy of at least 4 kJ/mol are shown in Figure 7. Examining the results, we note that there is only one configuration with a binding energy of 27 kJ/mol, approaching that of about 30 kJ/mol typically calculated[17] for HCl on ice I*h*; the next largest binding energy on a different NO_3^- group is only 14 kJ/mol, while H_2O and H_3O^+ chemical groups form only weak ∼10 kJ/mol hydrogen bonds with HCl. The variation in binding energy for a given chemical group (and between different chemical groups) is rationalized based on the different lengths of the H···O hydrogen bonds (which affects the strength of either the dipole−dipole or ion−dipole interactions), the

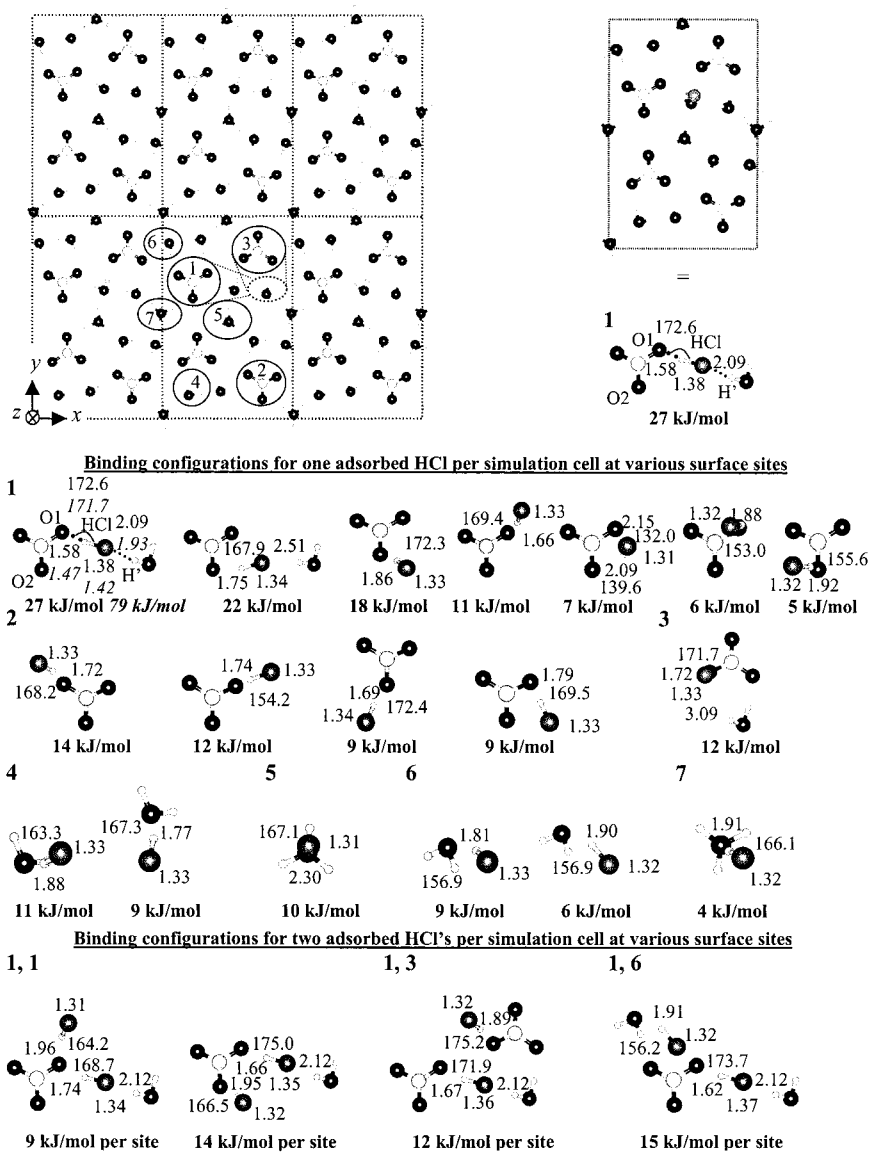

Figure 7. Optimized configurations of one HCl placed in 18 different configurations and two HCl's in four configurations on the NAT(001) face. Except for the most significant (27-kJ/mol) configuration, only chemical moieties involved in binding to HCl are shown; the rest of the face is omitted. Specified are $d_{HCl} = 1.31-1.42$ Å, $d_{O\cdots HCl} = 1.47-2.30$ Å, $\angle ClHO = 132.0-175.2°$, and $d_{Cl\cdots H'} = 2.09-3.09$ Å; italicized values were obtained with the LDA (as opposed to BLYP) functional. Binding energies at 0 K are specified with respect to HCl and the isolated slab, i.e., HCl + NAT → HCl·NAT or 2HCl + NAT → 2HCl·NAT, and are not corrected for zero-point energies, estimated to be −4 to −5 kJ/mol as described in the text.

different extents of surface distortion (relative to the isolated slab) that disrupt the surface bonding network, and (if applicable) the stabilizing influence of the Cl···H hydrogen bond. To gain further insight and examine the effect of increasing surface coverage, four additional two-adsorbate systems were generated (Figure 7), in each case by adding an HCl molecule to the HCl·NAT system with the largest binding energy, 27 kJ/mol. In two cases, the additional HCl molecule was placed on the same NO_3^- ion, in one case on a nearby NO_3^- ion, and in the final case on a nearby H_2O molecule. In all four cases, the average binding energy of the optimized two-adsorbate systems (9, 14, 12, and 15 kJ/mol) is less than the sum-average of the binding energies of the individual HCl·NAT systems, i.e., (27 + 11)/2 = 19, (27 + 18)/2 = 23, (27 + 12)/2 = 20, and (27 + 6)/2 = 17 kJ/mol. Equivalently, for each two-adsorbate configuration, the binding energy calculated for HCl at the second (additional) site is either only slightly positive (either 0 or 2 kJ/mol) or actually negative (either −8 or −5 kJ/mol). The difference between the average HCl binding energy and the sum-average of the individual HCl binding energies is smallest when the two HCl molecules are adsorbed on different chemical groups, as one would expect. We conclude that intramolecular sites near the 27-kJ/mol binding site compete very unfavorably for HCl, and that only one site on the (001) surface exhibits a high affinity for HCl.

The site that exhibits the greatest affinity for HCl on the (001) face involves the interaction of molecular HCl with a NO_3^- ion as well as with the dangling OH group of a nearby H_2O molecule. On the (100) face, there are two NO^- ions (per simulation cell) that would allow HCl to interact simultaneously with *two* dangling OH groups, forming a $NO_3^-\cdots HCl\cdots 2H_2O$ complex that would be less bent (and consequently more stable) than analogous complexes formed on other faces, i.e., (010). As observed on ice I*h*,[16,17] increasing the number of surface dangling OH groups may lead to a greater binding energy and ultimately partial dissociation of HCl. Two trial configurations of HCl at a binding site on the (100) face were optimized, with as before the surface lattice structure allowed to relax; the most

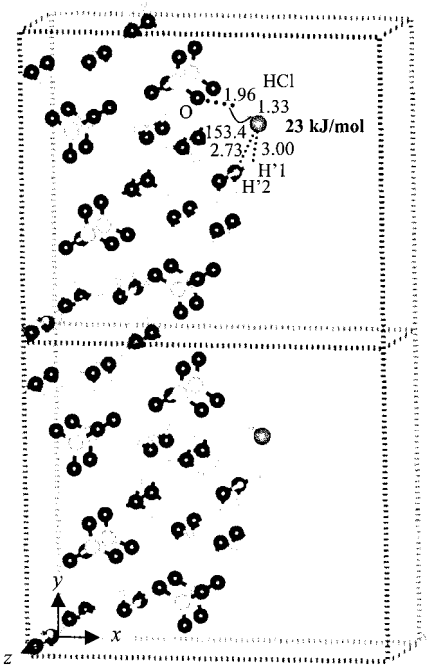

Figure 8. Optimized configuration of HCl placed on the NAT(100) face. For a slightly different initial placement of the HCl molecule, a second, less stable configuration resulted (with $d_{HCl} = 1.33$ Å, $d_{O\cdots HCl} = 2.09$ Å, $\angle ClHO = 148.4°$, $d_{Cl\cdots H'1} = 2.77$ Å, $d_{Cl\cdots H'2} = 2.40$ Å, and $-\Delta E_e^B = 9$ kJ/mol). See the caption of Figure 7 for additional details.

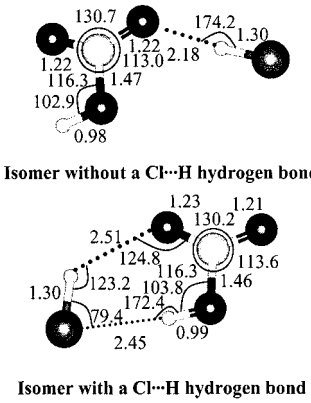

Figure 9. Optimized, isolated HNO_3·Cl complexes studied in order to estimate zero-point energy and thermal corrections to the binding energies in Figures 7 and 8.

stable optimized configuration is shown in Figure 8. The results in Figure 8 indicate that there are potential surface sites involving two dangling OH groups that show a high affinity for HCl. However, our 23-kJ/mol configuration involving two interacting dangling OH groups (Figure 8) is lower in energy than the 27-kJ/mol configuration depicted in Figure 7, despite the additional Cl···H hydrogen bond.

Before concluding this section, we note that in order to obtain binding energies or enthalpies at 190 K, a total correction (including zero-point energies) of either −5 to −4 kJ/mol or −3 to −2 kJ/mol, respectively, to the values in Figures 7 and 8 as the strength of the Cl···H hydrogen bond increases is estimated. These correction estimates are based on the actual corrections calculated for two gas-phase HNO_3·HCl complexes with the optimized structures at the BLYP level of theory with a 6-311++G(d,p) basis set shown in Figure 9. We note that our calculated corrections (and binding energies) for the HNO_3·HCl complexes are of the same order of magnitude as those

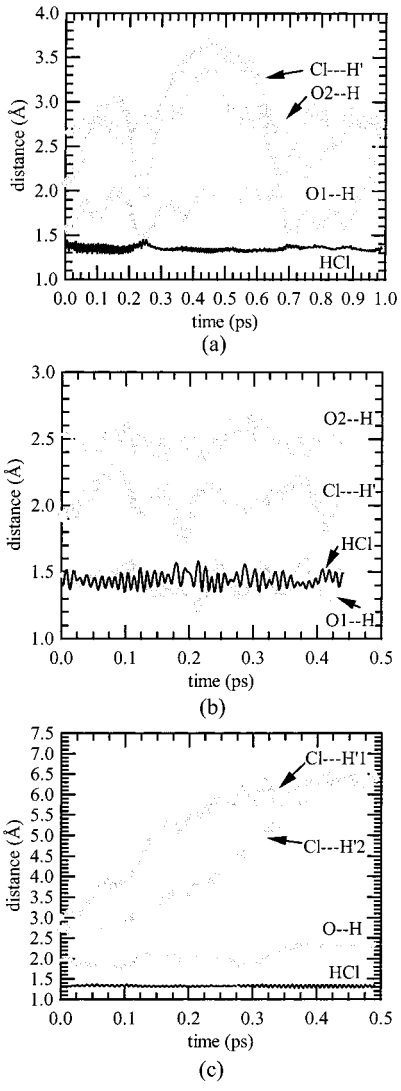

Figure 10. Evolution of atomic distances during three CPMD simulations at 155 K for (a) 0.99, (b) 0.44, or (c) 0.49 ps with HCl initially adsorbed at the (a) 27-kJ/mol (BLYP) or (b) 79-kJ/mol (LDA) binding site on the NAT(001) face (Figure 7), or at the (c) 23-kJ/mol (BLYP) binding site on the (100) face (Figure 8).

obtained in a recent theoretical study of the stability of hydrogen-bonded complexes of HNO_3 with various bases.[71]

C. Car-Parrinello Molecular Dynamics of Molecular HCl Adsorbed on NAT. To investigate the atmospheric fate of HCl, three CPMD simulations were performed (Figure 10). The first simulation was performed with HCl initially adsorbed at the 27-kJ/mol binding site with one dangling OH group on the (001) face. During this simulation, the HCl bond length does not change by more than several hundredths of an angstrom from its equilibrium value of 1.38 Å, and the HCl molecule remains hydrogen-bonded to the NO_3^- ion; however, the HCl molecule frequently breaks and re-forms its single Cl···H hydrogen bond with H_2O (Figure 10a). We emphasize that HCl forms at most a single Cl···H hydrogen bond at any time during the simulation, and always with the same H_2O molecule. Our results suggest that dissociation of adsorbed HCl on the (001) face is not kinetically rapid, although we note that only one trajectory was obtained, and it is possible (although not expected) that there are additional paths that are significant at $\gtrsim$1 ps time scales.

As the intermolecular atomic distances in Figure 10a imply, the (001) surface of NAT is quite dynamic and expands by 3−4 Å in the *c*-direction at 155 K. The expansion observed during

the simulation likely arises from the comparatively weaker hydrogen binding along the *c*-axis and the fact that the BLYP functional underestimates hydrogen bond strengths, e.g., that of $(H_2O)_2$.[57] To test this hypothesis, a second (otherwise identical) simulation was performed using the LDA functional. The intermolecular atomic distances are more "well behaved" (Figure 10b) and expansion is not observed, verifying our hypothesis. Sharing of the $H^{\delta+}$ of HCl between $Cl^{\delta-}$ and NO_3^- is observed during this simulation, although the HCl bond length (1.5 Å) is still considerably shorter than that obtained[16] with BLYP when HCl partially dissociates on ice I*h* when interacting with two dangling OH groups (1.8 Å). This sharing occurs because the H···O and Cl···H hydrogen bond strengths are likely overestimated, compensating for the fact that LDA yields D_e = 483 kJ/mol for HCl(g) → H(g) + Cl(g) compared to the BLYP value[16] of D_e = 421 kJ/mol and the experimental value[52,72] of D_o = 428 kJ/mol (an estimate of the experimental dissociation energy of adsorbed HCl on ice, which includes zero-point energies). Last, a third simulation was performed with HCl initially adsorbed at the 23-kJ/mol binding site with two dangling OH groups on the (100) face (Figure 8) using the BLYP functional. During the simulation, appreciable expansion of NAT along the *a*-axis is not observed. Interestingly, HCl does not interact with either dangling OH group (Figure 10c), preferring instead a perpendicular surface orientation, suggesting that dissociation of HCl on the (100) face is not kinetically rapid.

To test whether dissociation of adsorbed HCl on the NAT (001) face is thermodynamically favorable, the 27-kJ/mol binding site depicted in Figure 7 was modified by cleaving the HCl bond and forming an $O_2NOH\cdots Cl\cdots H_2O$ complex as part of the (001) surface (with d_{O_3N-H} = 1.00 Å, $d_{H\cdots Cl}$ = 1.96 Å, $d_{Cl\cdots H'}$ = 2.10 Å, and ∠OHCl = 174.8°). The HNO_3 comprising the $O_3NH\cdots Cl\cdots H_2O$ complex was nearly planar, with a geometry that was similar to gas-phase HNO_3, and was not significantly strained. A geometry optimization was subsequently performed. During the optimization, a single proton transfer was observed, reforming the 27-kJ/mol binding site with slightly different geometric parameters (i.e., $d_{O_3N\cdots H}$ = 1.56 Å, d_{HCl} = 1.38 Å, $d_{Cl\cdots H'}$ = 2.10 Å, and ∠OHCl = 172.9°) but the same binding energy, thereby demonstrating that (partially) dissociated HCl readily reforms molecular HCl at this binding site.

Last, to test whether dissociation of adsorbed HCl on the (100) face of NAT is thermodynamically favorable, the 23-kJ/mol binding site in Figure 8 was modified by cleaving the HCl bond and forming two $O_2NOH\cdots Cl\cdots(H_2O)_2$ complexes, one with Cl initially interacting most strongly with HNO_3 (i.e., $d_{H\cdots Cl}$ = 1.89 Å, $d_{Cl\cdots H'1} = d_{Cl\cdots H'2}$ = 2.85 Å) and one with Cl equidistant between the three hydrogen atoms (i.e., $d_{H\cdots Cl} = d_{Cl\cdots H'1} = d_{Cl\cdots H'2}$ = 2.44 Å). A geometry optimization of each complex was subsequently performed. The interaction energies (relative to the isolated molecule and slab) calculated for each optimized $O_2NOH\cdots Cl\cdots(H_2O)_2$ complex were −6 and 1 kJ/mol, respectively, and molecular HCl was not reformed. Consequently, we conclude that the $O_2NOH\cdots Cl\cdots(H_2O)_2$ complex is not thermodynamically likely relative to the 23-kJ/mol binding site in Figure 8. We do not rule out the (remote) possibility that there may be a nearby local minimum in which the $O_2NOH\cdots Cl\cdots(H_2O)_2$ complex is thermodynamically more stable. We also do not rule out the possibility of the existence of this complex in defect regions.

IV. Atmospheric Implications

As pointed out in the Introduction, experimental studies indicate that the surface coverage of HCl on "HNO_3-rich" NAT is likely at least 1 order of magnitude less than that measured on either of the forms of NAT intermediate between "HNO_3-rich" and "H_2O-rich" or on ice I*h*. This is consistent with our theoretical finding that only one adsorption site on the (likely prevalent) NAT(001) face results in appreciable binding, implying a lower surface coverage of HCl on "HNO_3-rich" NAT. Only one site on the NAT(001) face forms a hydrogen bond of appreciable energy (27 kJ/mol) with HCl, whereas on ice I*h* it was shown[17] that three sites on the ice I*h* (0001) face interact as strongly with HCl. Based on the dimensions of our PSC particle simulation cells, we estimate a saturated surface coverage of $\sigma_o = 1/(9.722\ \text{Å} \times 15.051\ \text{Å}) = 6.8 \times 10^{13}$ molecule/cm^2 on the NAT (001) face, but a larger value of $\sigma_o = 3/(9.046\ \text{Å} \times 9.046\ \text{Å} \times \sin 60°) = 4.2 \times 10^{14}$ molecule/cm^2 on the ice I*h* (0001) face. Note that we assume $\Delta H_{ads} \approx$ 25 kJ/mol for each surface in contrast to an early estimate of ∼74 kJ/mol on ice I*h* and "H_2O-rich" NAT and ∼54 kJ/mol on "HNO_3-rich" NAT.[73] We also are able to explain why the surface coverage on NAT approaches that on ice I*h* as the relative humidity increases: The number of adsorption sites on "H_2O-rich" NAT which are able to form a Cl···H hydrogen bond (with HCl and the dangling OH group of an H_2O molecule either adsorbed on or incorporated into the surface) will be greater.

An increased surface coverage of HCl on "H_2O-rich" NAT may explain at least partially the rate enhancement of chlorine activation on "H_2O-rich" NAT and water ice. Chlorine activation on "HNO_3-rich" NAT is still appreciable compared to the prohibitively slow gas-phase reaction between closed-shell molecules. Our results in Section IIIC suggest that molecular HCl adsorbed at the NAT surface is predominant. By contrast, two dangling OH groups at the ice I*h* (0001) face interacting strongly with adsorbed HCl induce partial dissociation that is both kinetically rapid and thermodynamically favorable.[16] While dissociation of adsorbed HCl is not expected at the "HNO_3-rich" NAT surface, other pathways for lowering the activation energy of reaction 3 are possible: HCl incorporation into the NAT bulk and subsequent ionization following the proposed mechanism on ice I*h* by Hynes and co-workers[11−13] (involving a concerted proton transfer) may be one mechanism. Other possibilities are that adsorbed HCl is partially dissociated via the interaction of adsorbed HCl with nearby dangling OH groups in NAT surface defect regions. On "H_2O-rich" NAT, HCl probably interacts with coadsorbed H_2O molecules. Additional theoretical studies are needed in order to verify these possibilities.

V. Conclusions

The NAT bulk and low index faces were modeled and characterized theoretically, and the adsorption and dynamics of HCl on (001) and (100) faces fully representative of the variety of adsorption sites on NAT were investigated. Only one site per simulation cell on the thermodynamically likely (001) face exhibits a high affinity for HCl, resulting in the formation of a $NO_3^-\cdots HCl\cdots H_2O$ surface binding complex, with an uncorrected binding energy of 27 kJ/mol and a binding energy and enthalpy at 190 K corrected for zero-point energies of 23 and 25 kJ/mol, respectively. The HCl surface coverage on the (001) face of "HNO_3-rich" NAT is estimated to be lower than that on "H_2O-rich" NAT and ice I*h*, qualitatively consistent with experimental studies of HCl uptake on these surfaces and rates of chlorine activation, i.e., reaction 3. A different site on the (100) face with two nearby dangling OH groups also exhibits a high affinity for HCl, resulting in a $NO_3^-\cdots HCl\cdots(H_2O)_2$ complex. However, during Car-Parrinello MD simulations at

either high-affinity site, dissociation of HCl is not observed, suggesting that a molecular form of adsorbed HCl is preferred kinetically. Additionally, calculations suggest that the molecular form is also preferred thermodynamically. Chlorine activation on NAT may occur solely as a result of HCl dissociation in the bulk, at surface defects, or in the presence of coadsorbed H_2O molecules (not considered in this study), in contrast to ice I*h*, for which HCl dissociation on/atop the (0001) face is also predicted.

Acknowledgment. This work was partially supported by the NASA Upper Atmospheric Research Program (Grant No. NAG5-8887). Y.A.M. acknowledges partial support from the MIT Center for Global Change Sciences. This work was partially supported by the National Computational Science Alliance under a Boston University MARINER/Alliance startup allocation (Project No. 60390) and under Proposal No. CTS990016Nr01 and CHE010020N and utilized the Boston University SGI/CRAY Origin2000 and the NCSA SGI/CRAY Origin2000, respectively.

References and Notes

(1) Seinfeld, J. H.; Pandis, S. N. *Atmospheric Chemistry and Physics: From Air Pollution to Climate Change*; Wiley: New York, 1998.

(2) Solomon, S. *Rev. Geophys.* **1999**, *37*, 275.

(3) Sander, S. P.; Friedl, R. R.; DeMore, W. B.; Golden, D. M.; Kurylo, M. J.; Hampson, R. F.; Huie, R. E.; Moortgat, G. K.; Ravishankara, A. R.; Kolb, C. E.; Molina, M. J. *Chemical Kinetics and Photochemical Data for Use in Stratospheric Modeling, Supplement to Evaluation 12: Update of Key Reactions*; Jet Propulsion Laboratory: Pasadena, CA, 2000.

(4) DeMore, W. B.; Sander, S. P.; Golden, D. M.; Hampson, R. F.; Kurylo, M. J.; Howard, C. J.; Ravishankara, A. R.; Kolb, C. E.; Molina, M. J. *Chemical Kinetics and Photochemical Data for Use in Stratospheric Modeling*; Jet Propulsion Laboratory: Pasadena, CA, 1997.

(5) Petrenko, V. F.; Whitworth, R. W. *Physics of Ice*; Oxford University Press: New York, 1999.

(6) Schaff, J. E.; Roberts, J. T. *J. Phys. Chem.* **1994**, *98*, 6900.

(7) Geiger, F. M.; Pibel, C. D.; Hicks, J. M. *J. Phys. Chem. B* **2001**, *105*, 4940.

(8) Bianco, R.; Hynes, J. T. *J. Phys. Chem. A* **1998**, *102*, 309.

(9) McNamara, J. P.; Hillier, I. H. *J. Phys. Chem. A* **1999**, *103*, 7310.

(10) Bianco, R.; Thompson, W. H.; Morita, A.; Hynes, J. T. *J. Phys. Chem. A* **2001**, *105*, 3132.

(11) Gertner, B. J.; Hynes, J. T. *Science* **1996**, *271*, 1563.

(12) Gertner, B. J.; Hynes, J. T. *Faraday Discuss.* **1998**, *110*, 301.

(13) Bianco, R.; Hynes, J. T. *J. Phys. Chem. A* **1999**, *103*, 3797.

(14) McNamara, J. P.; Tresadern, G.; Hillier, I. H. *J. Phys. Chem. A* **2000**, *104*, 4030.

(15) Molina, M. J. The probable role of stratospheric "ice" clouds: Heterogeneous chemistry of the "ozone hole". In *The Chemistry of the Atmosphere: Its Impact on Global Change*; Calvert, J. G., Ed.; Blackwell Scientific Publications: Oxford, 1994; p 27.

(16) Mantz, Y. A.; Geiger, F. M.; Molina, L. T.; Molina, M. J.; Trout, B. L. *Chem. Phys. Lett.* **2001**, *348*, 285.

(17) Mantz, Y. A.; Geiger, F. M.; Molina, L. T.; Molina, M. J.; Trout, B. L. *J. Phys. Chem. A* **2001**, *105*, 7037.

(18) Mantz, Y. A.; Geiger, F. M.; Molina, L. T.; Molina, M. J.; Trout, B. L. *J. Chem. Phys.* **2000**, *113*, 10733.

(19) Bolton, K.; Pettersson, J. B. C. *J. Am. Chem. Soc.* **2001**, *123*, 7360.

(20) Svanberg, M.; Pettersson, J. B. C.; Bolton, K. *J. Phys. Chem. A* **2000**, *104*, 5787.

(21) Mebel, A. M.; Morokuma, K. *J. Phys. Chem.* **1996**, *100*, 2985.

(22) Haas, B.-M.; Crellin, K. C.; Kuwata, K. T.; Okumura, M. *J. Phys. Chem.* **1994**, *98*, 6740.

(23) Van Doren, J. M.; Viggiano, A. A.; Morris, R. A. *J. Am. Chem. Soc.* **1994**, *116*, 6957.

(24) Hanson, D. R. *J. Phys. Chem.* **1995**, *99*, 13059.

(25) Sodeau, J. R.; Horn, A. B.; Banham, S. F.; Koch, T. G. *J. Phys. Chem.* **1995**, *99*, 6258.

(26) Horn, A. B.; Sodeau, J. R.; Roddis, T. B.; Williams, N. A. *J. Chem. Soc., Faraday Trans.* **1998**, *94*, 1721.

(27) Oppliger, R.; Allanic, A.; Rossi, M. J. *J. Phys. Chem. A* **1997**, *101*, 1903.

(28) Hanson, D.; Mauersberger, K. *Geophys. Res. Lett.* **1988**, *15*, 855.

(29) Worsnop, D. R.; Fox, L. E.; Zahniser, M. S.; Wofsy, S. C. *Science* **1993**, *259*, 71.

(30) Tolbert, M. A.; Toon, O. B. *Science* **2001**, *292*, 61.

(31) Abbatt, J. P. D.; Molina, M. J. *J. Phys. Chem.* **1992**, *96*, 7674.

(32) Barone, S. B.; Zondlo, M. A.; Tolbert, M. A. *J. Phys. Chem. A* **1997**, *101*, 8643.

(33) Henson, B. F.; Wilson, K. R.; Robinson, J. M. *Geophys. Res. Lett.* **1996**, *23*, 1021.

(34) Hanson, D. R.; Ravishankara, A. R. *J. Geophys. Res.* **1993**, *98D*, 22931.

(35) Carslaw, K. S.; Peter, T. *Geophys. Res. Lett.* **1997**, *24*, 1743.

(36) Peter, T. *Annu. Rev. Phys. Chem.* **1997**, *48*, 785.

(37) Chu, L. T.; Leu, M. T.; Keyser, L. F. *J. Phys. Chem.* **1993**, *97*, 7779.

(38) Lee, S.-H.; Leard, D. C.; Zhang, R.; Molina, L. T.; Molina, M. J. *Chem. Phys. Lett.* **1999**, *315*, 7.

(39) Leu, M.-T.; Keyser, L. F.; Timonen, R. S. *J. Phys. Chem. B* **1997**, *101*, 6259.

(40) Foster, K. L.; Tolbert, M. A.; George, S. M. *J. Phys. Chem. A* **1997**, *101*, 4979.

(41) Poshusta, R. D.; Tseng, D. C.; Hess, A. C.; McCarthy, M. I. *J. Phys. Chem.* **1993**, *97*, 7295.

(42) Tóth, G. *J. Phys. Chem. A* **1997**, *101*, 8871.

(43) Sulliven, D. M.; Bagchi, K.; Tuckerman, M. E.; Klein, M. L. *J. Phys. Chem. A* **1999**, *103*, 8678.

(44) Hutter, J.; Alavi, A.; Deutsch, T.; Bernasconi, M.; Goedecker, St.; Marx, D.; Tuckerman, M.; Parrinello, M. *CPMD*; Max-Planck Institut für Festkörperforschung and IBM Zurich Research Laboratory, 1995−99.

(45) Becke, A. D. *Phys. Rev. A* **1988**, *38*, 3098.

(46) Lee, C.; Yang, W.; Parr, R. G. *Phys. Rev. B* **1988**, *37*, 785.

(47) Goedecker, S.; Teter, M. P.; Hutter, J. *Phys. Rev. B* **1996**, *54*, 1703.

(48) Troullier, N.; Martins, J. L. *Phys. Rev. B* **1991**, *43*, 1993.

(49) Kirkpatrick, S.; Gelatt, C. D., Jr.; Vecchi, M. P. *Science* **1983**, *220*, 671.

(50) Frisch, M. J.; Trucks, G. W.; Schlegel, H. B.; Gill, P. M. W.; Johnson, B. G.; Robb, M. A.; Cheeseman, J. R.; Keith, T. A.; Petersson, G. A.; Montgomery, J. A.; Raghavachari, K.; Al-Laham, M. A.; Zakrzewski, V. G.; Ortiz, J. V.; Foresman, J. B.; Cioslowski, J.; Stefanov, B. B.; Nanayakkara, A.; Challacombe, M.; Peng, C. Y.; Ayala, P. Y.; Chen, W.; Wong, M. W.; Andres, J. L.; Replogle, E. S.; Gomperts, R.; Martin, R. L.; Fox, D. J.; Binkley, J. S.; Defrees, D. J.; Baker, J.; Stewart, J. P.; Head-Gordon, M.; Gonzalez, C.; Pople. J. A. *Gaussian 94 (Revision E.3)*; Gaussian, Inc.: Pittsburgh, PA, 1995.

(51) Wong, M. W. *Chem. Phys. Lett.* **1996**, *256*, 391.

(52) Huber, K. P.; Herzberg, G. *Molecular Spectra and Molecular Structure IV. Constants of Diatomic Molecules*; Van Nostrand: New York, 1979.

(53) McGraw, G. E.; Bernitt, D. L.; Hisatsune, I. C. *J. Chem. Phys.* **1965**, *42*, 237.

(54) Car, R.; Parrinello, M. *Phys. Rev. Lett.* **1985**, *55*, 2471.

(55) Marx, D.; Hutter, J. Ab initio molecular dynamics: Theory and implementation. In *Modern Methods and Algorithms of Quantum Chemistry*; Grotendorst, J., Ed.; John von Neumann Institute for Computing: Jülich, 2000; Vol. NIC Series, Vol. 1, p 301.

(56) Sugino, O.; Car, R. *Phys. Rev. Lett.* **1995**, *74*, 1823.

(57) Sprik, M.; Hutter, J.; Parrinello, M. *J. Chem. Phys.* **1996**, *105*, 1142.

(58) Tao, F.-M.; Higgins, K.; Klemperer, W.; Nelson, D. D. *Geophys. Res. Lett.* **1996**, *23*, 1797.

(59) Donaldson, D. J.; Orlando, J. J.; Amann, S.; Tyndall, G. S.; Proos, R. J.; Henry, B. R.; Vaida, V. *J. Phys. Chem. A* **1998**, *102*, 5171.

(60) Staikova, M.; Donaldson, D. J. *Phys. Chem. Chem. Phys.* **2001**, *3*, 1999.

(61) Canagaratna, M.; Phillips, J. A.; Ott, M. E.; Leopold, K. R. *J. Phys. Chem. A* **1998**, *102*, 1489.

(62) Cox, A. P.; Ellis, M. C.; Attfield, C. J.; Ferris, A. C. *J. Mol. Struct.* **1994**, *320*, 91.

(63) Benedict, W. S.; Gailer, N.; Plyler, E. K. *J. Chem. Phys.* **1956**, *24*, 1139.

(64) Taesler, I.; Delaplane, R. G.; Olovsson, I. *Acta Crystallogr.* **1975**, *B31*, 1489.

(65) Goto, A.; Hondah, T.; Mae, S. *J. Chem. Phys.* **1990**, *93*, 1412.

(66) Colbeck, S. C. *J. Cryst. Growth* **1985**, *72*, 726.

(67) Hobbs, P. V. *Ice Physics*; Clarendon Press: Oxford, 1974.

(68) Becke, A. D.; Edgecombe, K. E. *J. Chem. Phys.* **1990**, *92*, 5397.

(69) Trout, B. L.; Parrinello, M. *J. Phys. Chem. B* **1999**, *103*, 7340.

(70) Kroes, G.-J.; Clary, D. C. *J. Phys. Chem.* **1992**, *96*, 7079.

(71) Dimitrova, Y. *J. Mol. Struct. (THEOCHEM)* **2000**, *532*, 41.

(72) Dunning, T. H., Jr. *J. Phys. Chem.* **1984**, *88*, 2469.

(73) Tabazadeh, A.; Turco, R. P. *J. Geophys. Res.* **1993**, *98D*, 12727.